Arabian Journal of Chemistry (2023) 16, 104437

King Saud University

Arabian Journal of Chemistry

www.ksu.edu.sa
www.sciencedirect.com

ORIGINAL ARTICLE

Synthesis, anticancer evaluation, and molecular modeling study of new 2-(phenylamino)pyrazolo [1,5-*a*]pyrimidine analogues

Omer A. Azher [a], **Aisha Hossan** [b], **Rami A. Pashameah** [c], **Amerah Alsoliemy** [c], **Arwa Alharbi** [c], **Turki M. Habeebullah** [d], **Nashwa M. El-Metwaly** [c,e,*]

[a] *Department of laboratory Medicine, Faculty of Applied Biomedical Sciences, Al-Baha University, Saudi Arabia*
[b] *Department of Chemistry, Faculty of science, King Khalid University, Abha, Saudi Arabia*
[c] *Department of Chemistry, Faculty of Applied Science, Umm Al Qura University, Makkah 24230, Saudi Arabia*
[d] *Department of Environment and Health Research, The Custodian of the two holy mosques Institute for Hajj and Umrah Research, Umm Al Qura University, Makkah, Saudi Arabia*
[e] *Department of Chemistry, Faculty of Science, Mansoura University, El-Gomhoria Street 35516, Egypt*

Received 18 August 2022; accepted 13 November 2022
Available online 17 November 2022

KEYWORDS

3-aminopyrazoles;
Pyrazolopyrimidines;
Molecular modelling;
MCF-7;
Molecular docking

Abstract The reaction of 3-amino-5-phenylaminopyrazoles **2** with 3-(dimethylamino) acrylonitrile derivatives resulted in a series of substituted pyrazolopyrimidine analogues **4** and **6**. The DFT studies of the isolated compounds showed that the frontier molecular orbitals energy gap was close and in the 2.65–2.81 eV range where the derivative **6b** has the lowest and both of **4a** and **4c** have the highest values. Meanwhile, the anticancer activity of the newly synthesized pyrazolopyrimidine analogues have been tested against several different cell lines (MCF-7, PC3, Hep-2 and WI38). The investigated pyrazolopyrimidines showed remarkable cytotoxicity activity against the MCF-7 and Hep-2 cell lines. In comparison to the effects of 5-fluorouracil, IC_{50} = 10.19 ± 0.42 and 7.19 ± 0.47, compounds **6a-c** demonstrated potential anticancer activity with IC_{50} values for MCF-7 (10.80 ± 0.36–19.84 ± 0.49 µM) and Hep-2 (8.85 ± 0.24–12.76 ± 0.16 µM). Important details regarding the protein's binding sites were disclosed when the produced analogues docked with the crystal structure of the KDM5A protein, which was located in the protein data library.

* Corresponding author.
E-mail addresses: oazher@bu.edu.sa (O.A. Azher), ahossan@kku.edu.sa (A. Hossan), rapasha@uqu.edu.sa (R.A. Pashameah), amsolieme@uqu.edu.sa (A. Alsoliemy), awharbi@uqu.edu.sa (A. Alharbi), tmhabeebullah@uqu.edu.sa (T.M. Habeebullah), N_elmetwaly00@yahoo.comnmm, nmmohamed@uqu.edu.sa (N.M. El-Metwaly).
Peer review under responsibility of King Saud University.

ELSEVIER Production and hosting by Elsevier

https://doi.org/10.1016/j.arabjc.2022.104437
1878-5352

1. Introduction

A significant heterocyclic moiety, the pyrimidine moiety exhibits a wide range of biological and pharmacological activity (Sathisha, Gopala et al. 2016, Jubeen, Iqbal et al. 2018, Nerkar 2021). Nucleotides, nucleic acids, vitamins, coenzymes, purines, pterins, and uric acids are examples of naturally occurring molecules that contain this six-membered 1,3-diazine ring with nitrogen at the 1 and 3 positions (Johnson and Khan 2018). The numerous medicinal uses of pyrimidine may be explained by the fact that it is a component of DNA and RNA (Joshi, Nayyar et al. 2016, Taylor, Houlihan et al. 2019). The first analogues to be examined for biological action were 5-halogenated analogues of pyrimidine moiety (Alcolea Palafox 2014, Matyugina, Logashenko et al. 2015). This heterocyclic moiety is part of several drugs like a fused, stiff, and planar *N*-heterocyclic system that contains both of pyrazole and pyrimidine moieties is known as the pyrazolo[1,5-*a*]pyrimidine (PP) (Arias-Gómez, Godoy et al. 2021, Mahapatra, Prasad et al. 2021). Due to its exceptional synthetic flexibility, this fused pyrazole is a preferred scaffold for combinatorial library design and drug discovery (Mackman, Sangi et al. 2015, Shirvani, Fassihi et al. 2019). This elasticity enables structural modifications all the way around its border. After the chief critical evaluation involving this interesting scaffold (Jismy, Tikad et al. 2020), several reviews regarding to the achievement and subsequent derivatization procedures have been designated in the literature (El Sayed, Hussein et al. 2018, Pinheiro et al. 2020, Kumar, Das et al. 2021). In spite of these discoveries, the synthetic alterations covering this theme continue to be an exploration in terms of the effectiveness of the development, the influence on the setting, and the investigation of its various uses. The methods that aim to shorten synthesis routes, use affordable reagents, and create waste-prevention or -reduction techniques should be covered in these studies. Typically, the preparation of PP analogues includes the formation of pyrimidine rings by reaction with various 1,3-biselectrophilic reagents with aminopyrazoles (Castillo and Portilla 2018, Al-Azmi 2019, Salem, Helal et al. 2019). Pyrazolo[1,5-*a*]pyrimidine analogues is considered an important fragment for bioactive materials through their unique properties corresponding to selectivity as a protein inhibitor (Asano, Yamazaki et al. 2012), anticancer (Zhao, Ren et al. 2016), between others outstanding qualities (Lunagariya, Thakor et al. 2018, Ali, Ibrahim et al. 2019, Almehmadi, Alsaedi et al. 2021). Additionally, the pyrazolo[1,5-*a*] pyrimidine biocompatibility and lower toxicity resulted in a wide range derivatives to be employed as bioactive materials under commercial names like "Zaleplon, Indiplon, Lorediplon, Reversan, Dorsomor-

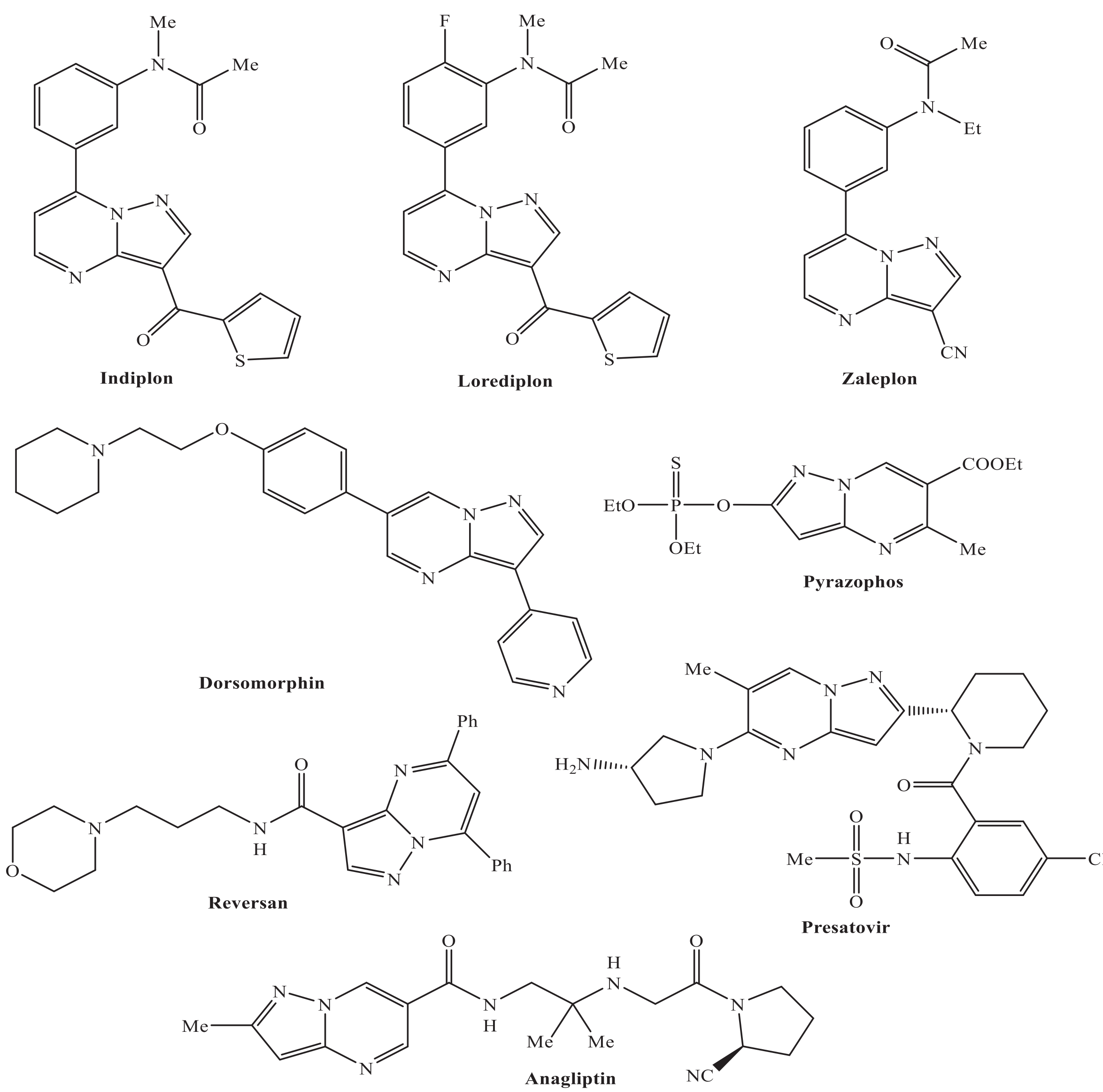

Fig. 1 Chemical structures of some derivatives bearing pyrazolopyrimidine motif.

phin, Pyrazophos, Anagliptin, and Presatovir" (Fig. 1) (Eftekhari-Sis and Zirak 2015). Recently, this molecular component has been the subject of research for potential new uses in the field of materials sciences, because of its outstanding photophysical characteristics as an emerging fluorophore (Castillo, Rosero et al. 2017, Tigreros, Aranzazu et al. 2020, Tigreros, Macias et al. 2021, Tigreros, Zapata-Rivera et al. 2021). Similarly, the propensity of pyrazolo[1,5-*a*]pyrimidine analogues to take the crystalline shapes with prominent conformations and supramolecular behaviors (Secrieru, O'Neill et al. 2019, Tigreros, Macías et al. 2022) could magnify their uses against the solid-state. From the previous literatures as substituted PPs presented good bioactivity, it encouraged us to synthesis another PP substituted with different groups such as substituted amide, substituted amino, and nitrile groups besides study their anticancer activities toward different cell lines in addition to study their theoretical activity through modeling and docking stimulation toward cancer protein.

2. Experimental

2.1. General remarks

Melting point measurements are performed using the Gallenkamp electric apparatus. The IR spectra were captured using a Thermo Scientific Nicolet iS10 FTIR spectrometer (KBr discs). The NMR spectra were obtained in DMSO d_6 using a JEOL NMR spectrometer at 500 MHz (^{1}H NMR) and 125 MHz (^{13}C NMR). The mass analyses were carried out on a Thermo Scientific Focus/DSQII Quadrupole GC/MS (70 eV). The C, H, and N elemental analyses were carried out using a Perkin-Elmer 2400 analyzer.

2.2. Preparation of 3-amino-N-aryl-5-(phenylamino)-1H-pyrazole-4-carboxamide analogues **2a-c**

Hydrazine hydrate 80 % (1.00 ml, 20 mmol) was added to each solution of the ketene *S*,*N*-acetal derivative **1a**, **1b**, or **1c** (15 mmol) in 40 ml of ethanol. The mixture in each case was heated under reflux for 6 h and the precipitated solid was filtered to pick up the targeting 3-amino-5-phenylamino-pyrazole derivatives **2a**, **2b**, and **2c**, respectively (Elgemeie, Elghandour et al. 2004, Elgemeie and Jones 2004, Mukhtar, Hassan et al. 2021).

2.3. Preparation of 7-amino-N-aryl-6-cyano-2-(phenylamino)-pyrazolo[1,5-a]pyrimidine-3-carboxamide analogues **4a-c**

To a solution of 3-amino-5-phenylamino-pyrazole derivative **2a**, **2b**, or **2c** (5 mmol) in 40 ml dioxane and 0.2 ml triethylamine, 2-((dimethylamino)methylene)-malononitrile (**3**) (0.60 g, 5 mmol) was added. The solution was heated under reflux for 3–4 h, the progress of the reaction was monitored by TLC. After completion of the reaction, the mixture was cooled to 30 °C. Crystallization of the obtained solid from a dioxane yielded the conforming pyrazolo[1,5-*a*]pyrimidine analogues **4a**, **4b**, and **4c**, respectively.

7-Amino-6-cyano-2-(phenylamino)-*N*-(*p*-tolyl)pyrazolo[1,5-*a*]pyrimidine-3-carboxamide (4a):

Yellow crystals, yield = 71 %, m.p. = 222–223 °C, R_f = 0.43 (hexane:EtOAc = 3:1). IR (ν/cm^{-1}): 3343, 3305, 3267, and 3190 (NH_2 and 2 N—H), 3056 (C—H, aromatic), 2941 (C—H, aliphatic), 2210 (C≡N), 1661 (C═O). ^{1}H NMR (*δ*/ppm): 2.29 (s, 3H, –CH_3), 6.87 (s, 2H, exchangeable by D_2O, NH_2), 7.14 (t, *J* = 7.50 Hz, 1H), 7.31 (d, *J* = 8.50 Hz, 2H), 7.40 (t, *J* = 8.50 Hz, 2H), 7.46 (d, *J* = 8.50 Hz, 2H), 7.58 (d, *J* = 8.50 Hz, 2H), 8.58 (s, 1H, pyrimidine-H), 10.25 (s, 1H, exchangeable by D_2O, N—H), 11.68 (s, 1H, exchangeable by D_2O, N—H). ^{13}C NMR (*δ*/ppm): 21.31 (–CH_3), 91.08 (C-6), 98.14 (C-3), 116.82 (C≡N), 118.64 (2 Ph-C), 121.11 (2 Ar-C), 123.54 (Ph-C), 129.35 (2 Ar-C), 129.98 (2 Ph-C), 134.67 (Ar-C), 136.70 (Ar-C), 139.96 (Ph-C), 151.38 (fused-C), 155.19 (C-2), 160.47 (C-5), 162.86 (C═O), 166.23 (C-7). MS *m*/*z* (%): 383 (M^+, 27.80). Analysis for $C_{21}H_{17}N_7O$ (383.15): Calcd.: C, 65.79; H, 4.47; N, 25.57 %. Found: C, 65.91; H, 4.41; N, 25.65 %.

7-Amino- *N*-(*p*-anisyl)-6-cyano-2-(phenylamino)pyrazolo[1,5-*a*]pyrimidine-3-carboxamide (4b):

Yellow crystals, yield = 65 %, m.p. = 230–231 °C, R_f = 0.54 (hexane:EtOAc = 3:1). IR (ν/cm^{-1}): 3332, 3294, 3245, and 3192 (NH_2 and 2 N—H), 3067 (C—H, aromatic), 2951 (C—H, aliphatic), 2211 (C≡N), 1658 (C═O). ^{1}H NMR (*δ*/ppm): 3.79 (s, 3H, –OCH_3), 6.91 (s, 2H, exchangeable by D_2O, NH_2), 7.04 (d, *J* = 9.00 Hz, 2H), 7.19 (t, *J* = 7.50 Hz, 1H), 7.46 (t, *J* = 7.50 Hz, 2H), 7.56 (d, *J* = 9.00 Hz, 2H), 7.75 (d, *J* = 9.00 Hz, 2H), 8.62 (s, 1H, pyrimidine-H), 10.43 (s, 1H, exchangeable by D_2O, N—H), 11.56 (s, 1H, exchangeable by D_2O, N—H). ^{13}C NMR (*δ*/ppm): 56.04 (–OCH_3), 90.87 (C-6), 97.44 (C-3), 114.91 (2 Ar-C), 116.57 (C≡N), 118.69 (2 Ph-C), 122.42 (2 Ar-C), 123.58 (Ph-C), 130.04 (2 Ph-C), 132.63 (Ar-C), 140.18 (Ph-C), 151.75 (fused-C), 154.80 (C-2), 159.05 (Ar-C), 161.17 (C-5), 163.24 (C═O), 165.89 (C-7). MS *m*/*z* (%): 399 (M^+, 43.29). Analysis for $C_{21}H_{17}N_7O_2$ (399.14): Calcd.: C, 63.15; H, 4.29; N, 24.55 %. Found: C, 63.01; H, 4.22; N, 24.44 %.

7-Amino-*N*-(*p*-chlorophenyl)-6-cyano-2-(phenylamino)pyrazolo[1,5-*a*]pyrimidine-3-carboxamide (4c):

Yellowish brown crystals, yield = 68 %, m.p. = 243–244 °C, R_f = 0.46 (hexane:EtOAc = 3:2). IR (ν/cm^{-1}): 3343, 3276, 3202 (NH_2 and 2 N—H), 3083 (C—H, aromatic), 2214 (C≡N), 1665 (C═O). ^{1}H NMR (*δ*/ppm): 6.94 (s, 2H, exchangeable by D_2O, NH_2), 7.13 (t, *J* = 7.50 Hz, 1H), 7.34 (t, *J* = 7.50 Hz, 2H), 7.48 (d, *J* = 9.00 Hz, 2H), 7.56 (d, *J* = 9.00 Hz, 2H), 7.70 (d, *J* = 7.50 Hz, 2H), 8.60 (s, 1H, pyrimidine-H), 10.41 (s, 1H, exchangeable by D_2O, N—H), 10.94 (s, 1H, exchangeable by D_2O, N—H). ^{13}C NMR (*δ*/ppm): 90.38 (C-6), 98.87 (C-3), 116.43 (C≡N), 118.55 (2 Ph-C), 121.69 (2 Ar-C), 123.30 (Ph-C), 128.85 (2 Ar-C), 129.81 (2 Ph-C), 133.17 (Ar-C), 135.93 (Ar-C), 139.49 (Ph-C), 152.07 (fused-C), 155.66 (C-2), 161.89 (C-5), 162.52 (C═O), 166.14 (C-7). MS *m*/*z* (%): 403 (M^+, 36.54). Analysis for $C_{20}H_{14}ClN_7O$ (403.09): Calcd.: C, 59.49; H, 3.49; N, 24.28 %. Found: C, 59.67; H, 3.44; N, 24.15 %.

2.4. Synthesis of 7-amino-N_3-aryl-2-(phenylamino)-pyrazolo[1,5-a]pyrimidine-3,6-dicarboxamide analogues **6a-c**

A mixture of each 3-aminopyrazole compound **2a**, **2b**, or **2c** (5 mmol) 2-cyano-3-(dimethylamino)acrylamide (**5**) (0.69 g, 5 mmol) in 30 ml dioxane and 0.2 ml triethylamine was heated under reflux for 3–4 h. The progress of the reaction was monitored by TLC. After completion of the reaction, the solid that obtained upon cooling to 30 °C was filtered and crystallized EtOH/DMF mixture (2:1) to give the corresponding pyrazolo[1,5-*a*]pyrimidine analogues **6a**, **6b**, and **6c**, respectively.

7-Amino-2-(phenylamino)–N_3-(*p*-tolyl)pyrazolo[1,5-*a*] pyrimidine-3,6-dicarboxamide (6a):

Orange crystals, yield = 62 %, m.p. = 265–266 °C, R_f = 0.33 (hexane:EtOAc = 1:1). IR (ν/cm^{-1}): 3369, 3311, 3260, 3194 (NH_2 and 2 N—H), 3062 (C—H, aromatic), 2938 (C—H, aliphatic), 1658 (C═O). ^{1}H NMR (*δ*/ppm): 2.32 (s, 3H, –CH_3), 6.70 (s, 2H, exchangeable by D_2O, NH_2), 7.07 (t, *J* = 7.50 Hz, 1H), 7.28–7.35 (m, 4H), 7.44 (d, *J* = 8.50 Hz, 2H), 7.57 (d, *J* = 8.50 Hz, 2H), 7.88 (s, 2H, exchangeable by D_2O, NH_2), 8.18 (s, 1H, pyrimidine-H), 10.52 (s, 1H, exchangeable by D_2O, N—H), 11.37 (s, 1H, exchangeable by D_2O, N—H). ^{13}C NMR (*δ*/ppm): 21.33 (–CH_3), 98.51 (C-3), 104.29 (C-6), 118.78 (2 Ph-C), 120.93 (2 Ar-C), 123.47 (Ph-C), 129.27 (2 Ar-C), 129.97 (2 Ph-C), 135.48 (Ar-C), 136.17 (Ar-C), 140.36 (Ph-C), 143.62 (fused-C), 155.39 (C-2), 158.96 (C-5), 163.21 (C═O), 165.56 (C-7), 167.09 (C═O). MS *m/z* (%): 401 (M^+, 67.11). Analysis for $C_{21}H_{19}N_7O_2$ (401.16): Calcd.: C, 62.83; H, 4.77; N, 24.42 %. Found: C, 62.94; H, 4.69; N, 24.50 %.

7-Amino-N_3–(*p*-anisyl)-2-(phenylamino)pyrazolo[1,5-*a*] pyrimidine-3,6-dicarboxamide (6b):

Brown powder, yield = 60 %, m.p. = 271–272 °C, R_f = 0.41 (hexane:EtOAc = 1:2). IR (ν/cm^{-1}): 3337, 3282, 3229 (NH_2 and 2 N—H), 3078 (C—H, aromatic), 2954 (C—H, aliphatic), 1655 (C═O). ^{1}H NMR (*δ*/ppm): 3.81 (s, 3H, –OCH_3), 7.01 (d, *J* = 9.00 Hz, 2H), 7.07 (s, 2H, exchangeable by D_2O, NH_2), 7.17 (t, *J* = 7.50 Hz, 1H), 7.38 (d, *J* = 7.50 Hz, 2H), 7.56 (t, *J* = 7.50 Hz, 2H), 7.72 (d, *J* = 9.00 Hz, 2H), 7.88 (s, 2H, exchangeable by D_2O, NH_2), 8.21 (s, 1H, pyrimidine-H), 10.26 (s, 1H, exchangeable by D_2O, N—H), 11.11 (s, 1H, exchangeable by D_2O, N—H). ^{13}C NMR (*δ*/ppm): 56.05 (–OCH_3), 97.85 (C-3), 103.02 (C-6), 114.56 (2 Ar-C), 119.07 (2 Ph-C), 122.44 (2 Ar-C), 123.54 (Ph-C), 129.81 (2 Ph-C), 130.69 (Ar-C), 139.86 (Ph-C), 143.73 (fused-C), 154.98 (C-2), 158.46 (Ar-C), 159.13 (C-5), 163.05 (C═O), 164.82 (C-7), 166.95 (C═O). MS *m/z* (%): 417 (M^+, 55.08). Analysis for $C_{21}H_{19}N_7O_3$ (417.15): Calcd.: C, 60.42; H, 4.59; N, 23.49 %. Found: C, 60.21; H, 4.48; N, 23.63 %.

7-Amino-N_3–(*p*-chlorophenyl)-2-(phenylamino)pyrazolo[1, 5-*a*]pyrimidine-3,6-dicarboxamide (6c):

Brown powder, yield = 58 %, m.p. = 293–294 °C, R_f = 0.45 (hexane:EtOAc = 1:2). IR (ν/cm^{-1}): 3351, 3307, 3266, 3208 (NH_2 and 2 N—H), 3087 (C—H, aromatic), 1657 (C═O). ^{1}H NMR (*δ*/ppm): 6.79 (s, 2H, exchangeable by D_2O, NH_2), 7.09 (t, *J* = 7.50 Hz, 1H), 7.28 (d, *J* = 8.50 Hz, 2H), 7.33–7.38 (m, 4H), 7.63 (d, *J* = 8.50 Hz, 2H), 7.67 (s, 2H, exchangeable by D_2O, NH_2), 8.24 (s, 1H, pyrimidine-H), 10.58 (s, 1H, exchangeable by D_2O, N—H), 11.46 (s, 1H, exchangeable by D_2O, N—H). ^{13}C NMR (*δ*/ppm): 98.77 (C-3), 105.43 (C-6), 118.81 (2 Ph-C), 121.89 (2 Ar-C), 123.63 (Ph-C), 129.18 (2 Ar-C), 129.78 (2 Ph-C), 133.05 (Ar-C), 135.92 (Ar-C), 140.43 (Ph-C), 144.07 (fused-C), 156.70 (C-2), 158.56 (C-5), 162.91 (C═O), 165.12 (C-7), 167.25 (C═O). MS *m/z* (%): 423 (M^+ + 2, 16.94), 421 (M^+, 48.32). Analysis for $C_{20}H_{16}ClN_7O_2$ (421.11): Calcd.: C, 56.95; H, 3.82; N, 23.24 %. Found: C, 57.13; H, 3.89; N, 23.36 %.

2.5. Computational studies

The produced compounds were geometrically optimized using Gaussian 09 W program (Frisch, Trucks et al. 2009) at DFT/B3LYP level and 6–311^{++}G basis set (Lee, Yang et al. 1988, Perdew and Wang 1992, Becke 1993). Positive frequencies obtained for all derivatives were taken as evidence for the optimized geometries stability. The Materials Studio package DMol3 module (BIOVIA 2017) was employed for estimating the Fukui indices by applying the GGA and B3LYP functional methods with DNP basis set (version 3.5) (Delley 2006).

2.6. MTT assay

The produced pyrazolo[1,5-*a*]pyrimidine derivatives were tested for their ability to suppress the growth of the subsequent cancer cell lines: liver carcinoma (HepG2), laryngeal carcinoma (Hep-2), breast cancer (MCF-7), and prostate cancer PC3. Normal fibroblast cells were also used in the MTT test (WI38). In this test, a colorimetric method is used to change the yellow hue of "tetrazolium bromide" (MTT) into a purple formazan by utilizing mitochondrial succinate dehydrogenase. Cell lines were bred in the meantime using RPMI-1640 media with 10 % bovine serum at 37 °C with 5 % CO_2. Next incubation for 24 hrs., cells were uncovered to various concentrations of the produced hybrids. After this, the cells were brooded for a further 4 h before receiving 5 mg/ml of MTT thaw, Liquefaction of the produced purple formazan**.**

2.7. Molecular docking study

The estimation of molecular docking was carried out using the molecular docking application (MOE 2015.10). We obtained the PDB for the KDM5A structure from (https://www.rcsb.org/PDB codes- 5IVE). The following instructions were followed for arranging the produced protein. i) The structure of the enzyme is cleaned up of objective substances. ii) The MOE method allowed hydrogen atoms to be added to protein while minimizing process, with RMS values of 0.01 kcal.mol^{-1} and an RMS range of 0.1. iii) The ligands were produced using the MOE builder interface.

3. Results and discussion

*3.1. Preparation of 2-(phenylamino)pyrazolo[1,5-**a**]pyrimidine analogues 4 and 6*

In light of the previous literature (Elgemeie, Elghandour et al. 2004, Elgemeie and Jones 2004, Mukhtar, Hassan et al. 2021), the building block 3-aminopyrazole derivatives **2a-c** were prepared by reacting the ketene *S*,*N*-acetal compounds **1a-c** with hydrazine hydrate in boiling ethanol for 6 h (Scheme 1).

The aminopyrazole compounds **2a-c** are used as starting materials for the synthesis of various substituted pyrazolo [1,5-*a*]pyrimidine analogues. They reacted with 2-((dimethylamino)methylene)-malononitrile (**3**) to form the 7-amino-*N*-aryl-6-cyano-2-(phenylamino)-pyrazolo[1,5-*a*]pyrimidine-3-carboxamide analogues **4a-c** (Scheme 2). The reaction was carried out by refluxing the reactants for 4 h in dioxane and triethylamine. The intermediate (**A**) is thought to be formed by the nucleophilic addition of an amino group (from pyrazole) to the β-carbon of acrylonitrile derivative **3**. This intermediate (**A**) undergoes dimethylamine molecule elimination, and the resulting intermediate (**B**) cyclizes to the pyrimidine

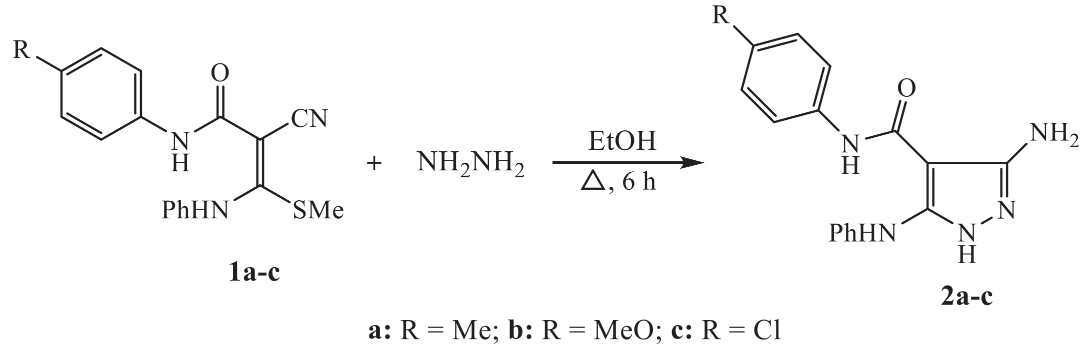

Scheme 1 Synthesis of 3-aminopyrazole scaffolds **2a-c**.

ring system via intramolecular addition of an internal N—H group (pyrazole) on the nitrile function. The structures of 7-aminopyrazolo[1,5-*a*]pyrimidine compounds **4a-c** were established by their compatible spectral data. The IR spectrum of **4a** (as an example) showed absorptions at 3343, 3305, 3267, and 3190 cm^{-1} referring to the NH_2 and 2 N—H stretching frequencies. The absorptions that observed 2210 and 1661 cm^{-1} were attributed to the nitrile (-C≡N), and amidic carbonyl (C═O) functions. ^{1}H NMR spectrum revealed singlet signals at δ 2.29 and 6.87 ppm for the protons of methyl and amino functions, respectively. The aromatic protons are resonated as triplet and doublet signals at in the region δ 7.14–7.58 ppm. The signal signals at δ 8.58, 10.25 and 11.68 ppm are attributed to the protons of pyrimidine-C and two N—H groups, respectively. The ^{13}C NMR spectrum revealed seventeen signals for twenty-one carbon atoms. The characteristic signals of pyrimidine-CH and amide carbonyl are observed at δ 160.47 and 162.86 ppm. The mass analysis showed the molecular ion peak at m/z = 383 for the formula $C_{21}H_{17}N_7O$.

The chemical reactivity of 3-aminopyrazoles **2a-c** with 2-cyano-3-(dimethylamino)acrylamide (**5**) was also studied. To obtain the targeting 2-(phenylamino)pyrazolo[1,5-*a*]pyrimidine-3,6-dicarboxamide compounds **6a-c**, the reaction was carried out in boiling dioxane and triethylamine (Scheme 3). The designed structures of compounds **6a-c** were confirmed by their compatible spectral data. The IR spectrum of **6a** showed absorptions at 3369, 3311, 3260, and 3194 cm^1 to indicate the stretching vibrations of NH_2 and two N—H groups. The amide carbonyl group is identified by the broad absorption near 1658 cm^{-1}. The ^{1}H NMR spectrum revealed singlet signals at δ 2.32 and 6.70 ppm for the protons of methyl and amino groups, respectively. The aromatic protons are observed as triplet, multiplet, and doublet signals at δ 7.07–7.57 ppm. The protons of amino group ($CONH_2$) are resonated as singlet at δ 7.88 ppm. The singlet signals that are resonated at δ 8.18, 10.52, and 11.37 ppm identified the pyrimidine-H and two N—H functions. The mass analysis showed the molecular ion peak at m/z = 401 for the formula $C_{21}H_{19}N_7O_2$.

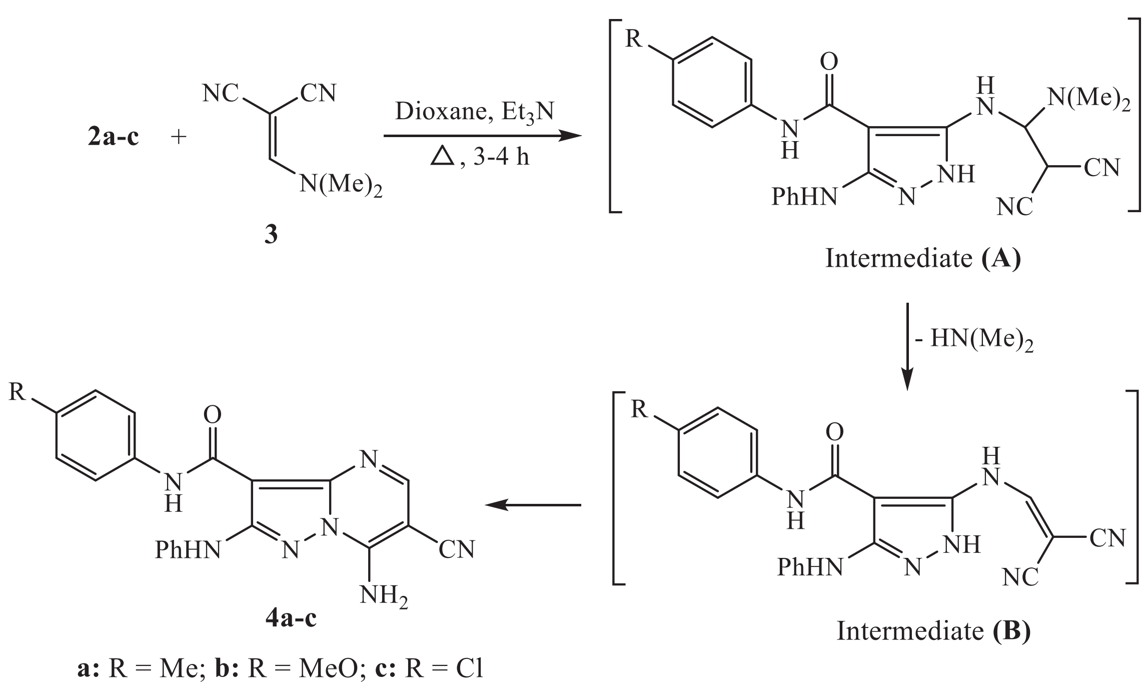

Scheme 2 Synthesis of 2-(phenylamino)pyrazolo[1,5-*a*]pyrimidine analogues **4a-c**.

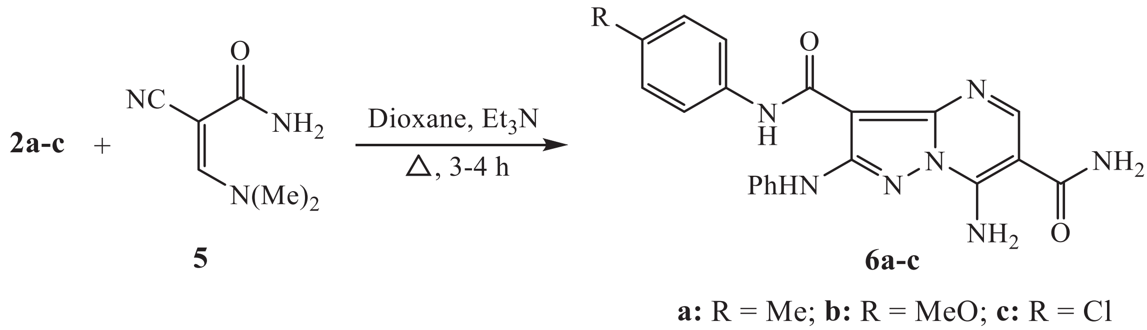

Scheme 3 Synthesis of 2-(phenylamino)pyrazolo[1,5-*a*]pyrimidine analogues **6a-c**.

3.2. DFT molecular modeling study

The studied compounds optimized structures revealed that the 2-phenylamino pyrazolopyrimidine moiety have almost planar configuration where the nitrogen atom of the phenylamino groups were slightly shifted out plane, $NH_{(Pham)}$–$C^2_{(Pp)}$-$N^1_{(Pp)}$-$N^8_{(Pp)}$ = 178.0° and $N^1_{(Pp)}$–$C^2_{(Pp)}$–$NH_{(Pham)}$-$C^1_{(Pham)}$ = 2.6°. Likewise, the amino and cyano substituents, in **4a-c** derivatives, were coplanar with the pyrazolopyrimidine, e.g., $NH_{2(Pp)}$-$C^7_{(Pp)}$-$C^6_{(Pp)}$-$C^5_{(Pp)}$ = -179.4°, $C^5_{(Pp)}$-$C^6_{(Pp)}$–$CN_{(Pp)}$–$NC_{(Pp)}$ = 179.3° and $NH_{2(Pp)}$-$C^7_{(Pp)}$-$C^6_{(Pp)}$–$CN_{(Pp)}$ = 0.4°. Although, the carboxamide carbonyl carbon atoms were out the pyrazolopyrimidine plane, e.g., $N^4_{(Pp)}$-$C^{3a}_{(Pp)}$–$C^3_{(Pp)}$–$CO_{(carb)}$ = 3.3°, whereas its oxygen and nitrogen atoms were strongly shifted out, i.e., $C^2_{(Pp)}$–$C^3_{(Pp)}$–$CO_{(carb)}$–$OC_{(carb)}$ and $C^2_{(Pp)}$–$C^3_{(Pp)}$–$CO_{(carb)}$–$NH_{(carb)}$ were −142.0° and 36.2°, respectively. In **6a-c** derivatives, the carboxamide group, at position 6, were slightly shifted out the pyrazolopyrimidine plane, e.g., $N^8_{(Pp)}$-$C^7_{(Pp)}$-$C^6_{(Pp)}$–$CO_{(carb1)}$ = -179.1°, $C^7_{(Pp)}$-$C^6_{(Pp)}$–$CO_{(carb1)}$–$OC_{(carb1)}$ = -2.0° and $C^5_{(Pp)}$-$C^6_{(Pp)}$–$CO_{(carb1)}$–$NH_{2(carb1)}$ = -1.9°. (Fig. 2) (Table S1).

Additionally, the DFT calculated bond length and angle were almost match with those measured in comparable compounds single crystal X-ray (Liu and Liao 2006, Xiaobao, Li et al. 2008, Burnett, Johnston et al. 2015), i.e., lengths exhibited 0.00–0.13 Å difference and 0.048–0.059 Å RMSD while the angles were different by 0.0–11.5° with 2.7–5.2° RMSD, which were attributed to the absence intermolecular columbic interactions in the quantum chemical calculations, but the practical gained for molecules in solid crystal lattice (Sajan, Joseph et al. 2011) (Tables S2-S3).

3.2.1. Frontier molecular orbitals

The HOMO-LUMO configuration and energy explain the electron donating or receiving ability of the molecule (Bulat, Chamorro et al. 2004) where lesser energy gap leads to more ease intramolecular charge transfer (Xavier, Periandy et al. 2015, Makhlouf, Radwan et al. 2018) that may affect in the molecule's biological activity (Bouchoucha, Zaater et al. 2018). The FMO 3D graph showed that the HOMO of all derivatives was localized mainly on the phenyl rings as well as the heteroatoms lone pair of electrons whilst the LUMO was principally constructed from the π*-orbitals of the 6-cyano and 6-carboxamide 3-carboxamide pyrazolopyrimidine moiety, in **4a-c** and **6a-c**, respectively (Fig. 3).(See Fig. 4).

The abovementioned facts affected in the HOMO-LUMO energies, E_H and E_L. So, the data indicated that the E_H and E_L of all derivatives have close values of the, range −5.65 - −6.18 and −3.06 - −3.37 eV, respectively, where **4c** has highest E_H and E_L. In addition, the derivatives **6b** and both of **4a** and **4c** exhibited the minimum and maximum $\Delta E_{H\text{-}L}$ gap, 2.59–2.81 eV, the compounds may be ordered according to their energy gap as **4a** = **4c** > **6c** ≈ **6a** > **4b** > **6b** (Table 1).

Furthermore, chemical reactivity descriptors, namely, electronegativity (χ), global hardness (η), softness (δ) and electrophilicity (ω) were determined utilizing the values of the E_H and E_L using the subsequent expressions (Xavier, Periandy et al. 2015).

$$\chi = -\frac{1}{2}(E_{HOMO} + E_{LUMO})\eta = -\frac{1}{2}(E_{HOMO} - E_{LUMO})$$

$$\delta = \frac{1}{\eta}\omega = \frac{\chi^2}{2\eta}$$

As shown in Table 1, from the electronegativity (χ) and global softness (δ) values, the derivative **6b** has minimum the Lewis's acid character and the maximum charge transfer ability, respectively. Thus, the examined derivatives were sorted, according to softness, as **6b** > **4b** > **6a** = **6c** > **4a** = **4c**. Furthermore, the molecule dipole moment (μ) accounts the intermolecular interactions where the higher the dipole moment, the stronger the intermolecular interactions will be. The dipole moments of the studied compounds were ranged from 0.86 to 8.17 D for compound **6b** and **4c**, respectively.

3.2.2. Atomic Mulliken's charges and Fukui's indices

The Mulliken's atomic charges shade light on the charge transfer and electronegativity properties of the molecule (Bhagyasree, Varghese et al. 2013). In all compounds, the pyrazolopyrimidine nitrogen atom $N^4_{(Pp)}$ has positive charge, 0.077–0.084. In contrast, the $N^1_{(Pp)}$ and $N^8_{(Pp)}$ have positive and negative charges, 0.045–0.098 and −0.031 - −0.082, respectively, in **4a-c** derivatives, while they possessed the opposite charges in **6a-c** derivatives. Noteworthy, the pyrazolopyrimidine carbon atom $C^7_{(Pp)}$ in the cyano derivatives, **4a-c**, have negative charge, −0.332 - −0.361, while in carboxamide derivatives, **6a-c**, it is positively charged, 0.161–0,266. Thus, this behavior may be attributed to the electron withdrawing effect of the cyano group in comparison to the carboxamide group. In contrary, the nitrogen atoms of the cyano and amine substituents in addition to the oxygen atoms of the carboxamide groups were negatively charged whereas the nitrogen atoms of both phenylamine and carboxamide in all compounds were acquired positive charge (Table 2).

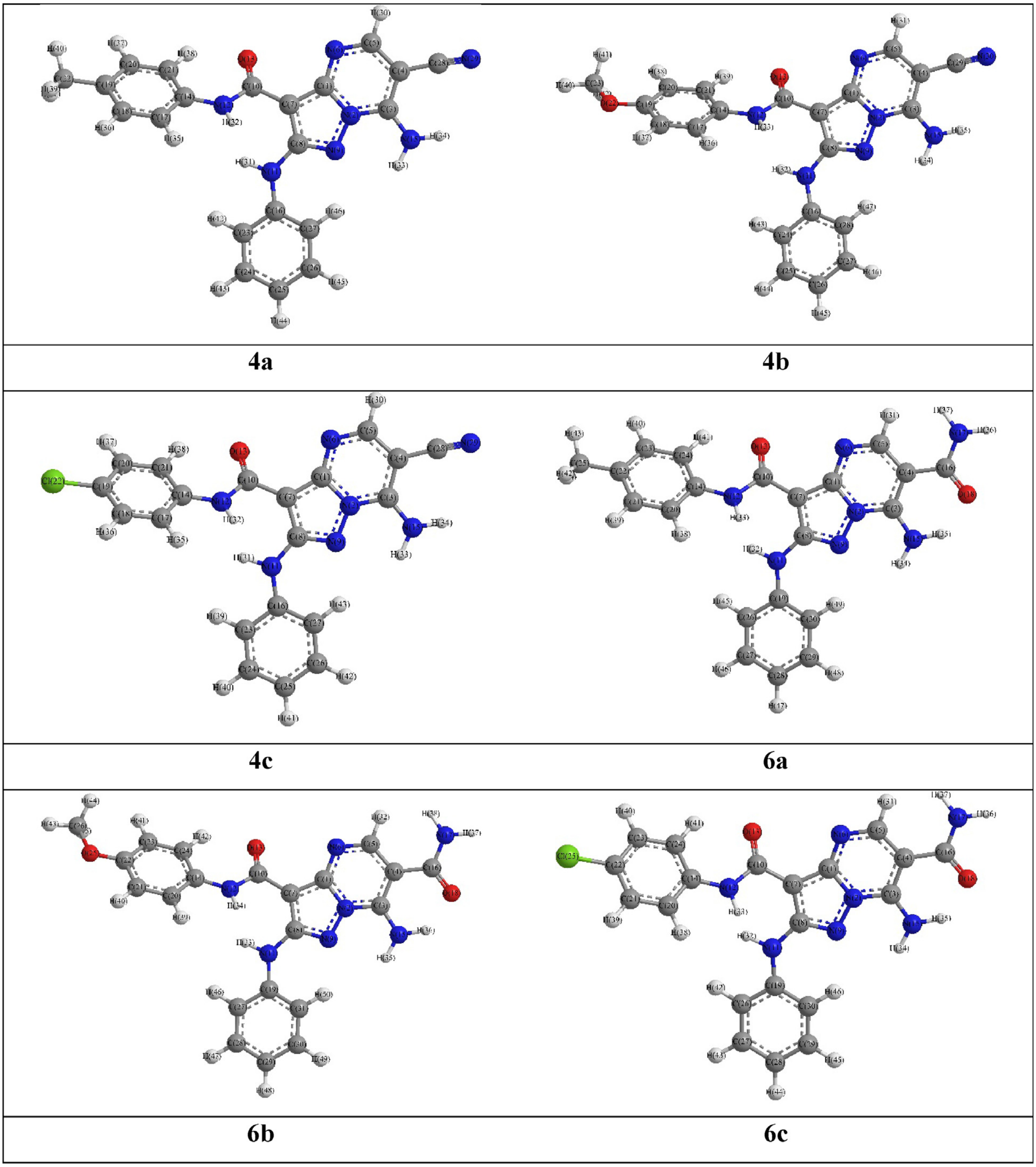

Fig. 2 DFT Optimized structures of the **4a** and **6a** derivatives.

Moreover, the Fukui's indices (f_k^+), as a measure of the atomic reactivity toward nucleophilic attack (El Adnani, Mcharfi et al. 2013, Mi, Xiao et al. 2015, Olasunkanmi, Obot et al. 2016, Messali, Larouj et al. 2018) (Table S4), revealed similar patterns, e.g., the derivatives **4a-c** showed that cyano nitrogen, $NC_{(Pp)}$, followed by the pyrazolopyrimidine carbon at positions 5 and 3a, $C^5_{(Pp)}$ and $C^{3a}_{(Pp)}$, while in **6a-c**, the carbon of the fused ring at position 5, $C^5_{(Pp)}$, occupied the top site followed by oxygen and carbon of the carboxamide group, $OC_{(carb1)}$ and $CO_{(carb1)}$, respectively (Table 3). Alternatively, the electrophilic attack Fukui's indices (f_k^-) presented close patterns for the highly susceptible atoms, e.g., in derivatives **4a** and **6a**, the carbon 4 and nitrogen atoms of the phenylamine group, $C^4_{(ph)}$ and $NH_{(Pham)}$, were occupied the second and third positions after cyano nitrogen atom, $NC_{(Pp)}$, in derivative **4a** while both were on the top in in derivative **6a**, respectively. Whereas, the methoxy derivatives **4b** and **6b** showed that the methoxy oxygen, $OMe_{(ph)}$, occupied the first place while the $C^1_{(ph)}$ and $C^4_{(ph)}$ atoms became the second and third susceptible sites, respectively. Lastly, the indices of radi-

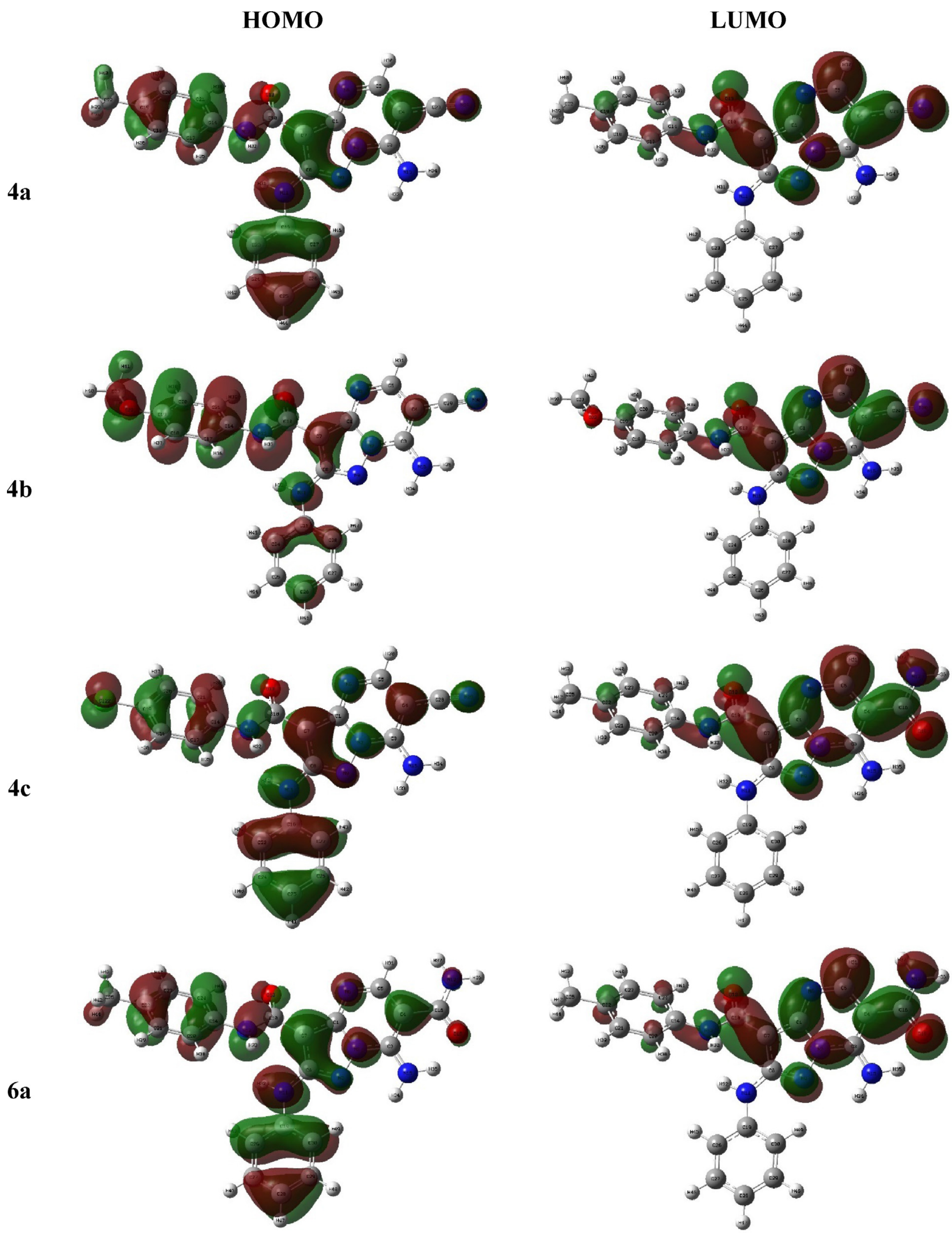

Fig. 3 The frontier molecular orbital of the investigated compounds.

cal attack (f_k^0) offered varied patterns, where in **4a-b**, the cyano nitrogen, $NC_{(Pp)}$, was on the top followed by the carbon 5 of the pyrazolopyrimidine, $C^5_{(Pp)}$, whereas, it occupied the first place in **6a-b** before the carboxamide oxygen, $OC_{(carb1)}$ (Table 3).(See Table 4).

As the Fukui's indices may be inaccurately predicted the active site for nucleophilic and electrophilic attack, the relative electrophilicity and nucleophilicity descriptors, s_k^-/s_k^+ and s_k^+/s_k^-, respectively, were calculated (Roy, de Proft et al. 1998, Roy, Krishnamurti et al. 1998, Roy, Pal et al. 1999),

6b

6c

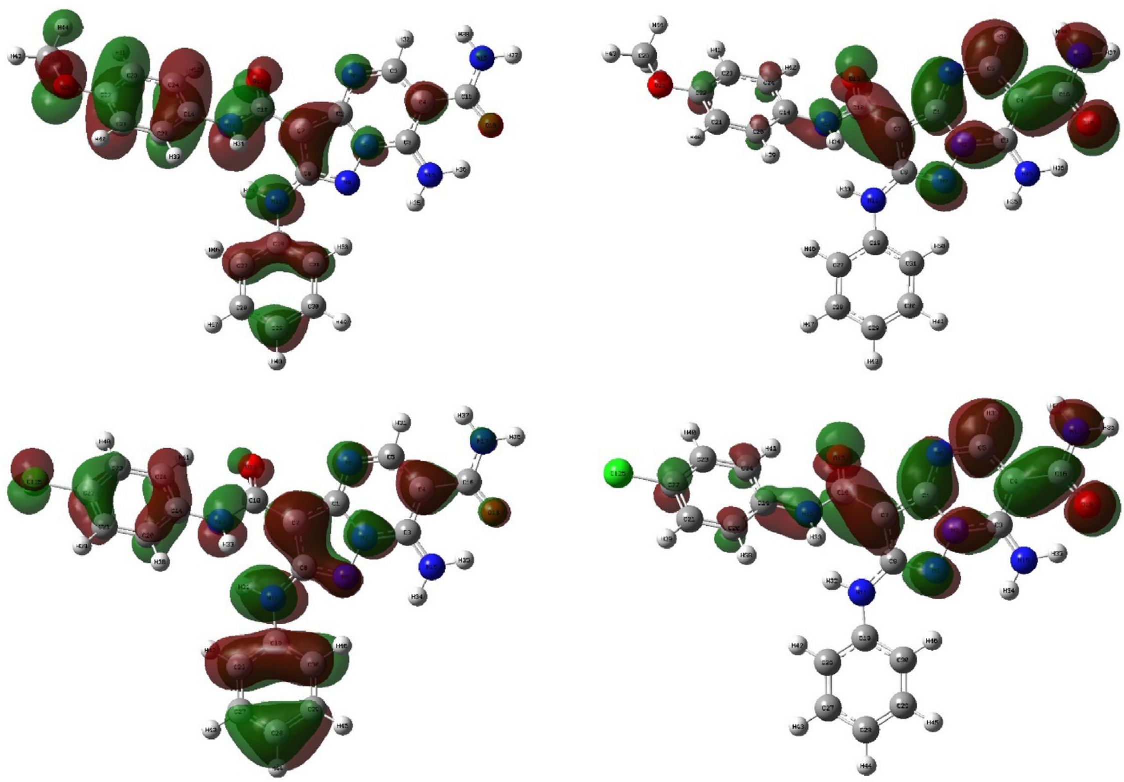

Fig. 3 (*continued*)

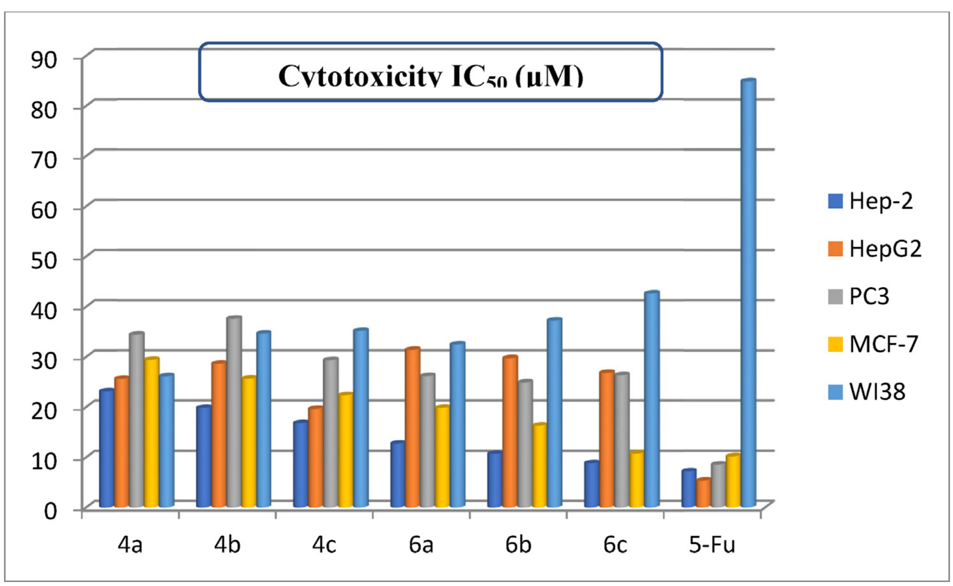

Fig. 4 IC$_{50}$ of the cytotoxic activity for the examined derivatives against human tumor cell lines.

where $s_k^+ = f_k^+ \times \delta$, $s_k^- = f_k^- \times \delta$ and δ is global softness (Table S4). The relative nucleophilicity descriptors data, s_k^+/s_k^-, presented resemble patterns, i.e., the **4a-c** derivatives exhibited the $C^5_{(Pp)}$ at the top position except **4c** in which the $CO_{(carb)}$ was the first. While, the **6a-c** derivatives displayed the $CO_{(carb1)}$ as the most active site followed by the $C^5_{(Pp)}$ (Table 3). As well, the relative electrophilicity descriptors, s_k^-/s_k^+, displayed that the phenyl carboxamide carbon $C^1_{(Phcarb)}$ atom was the most active site in all derivatives except **6a** and **6c** in which the phenylamine carbon $C^2_{(Pham)}$ was on the top. The second position was occupied by difference atoms, i.e., the phenylamine carbon $C^2_{(Pham)}$ presented in **4a**, **4c** and **6b**, while the **4b**, **6a** and **6c** have the $C^2_{(Phcarb)}$, $C^1_{(Pham)}$ and $C^1_{(Phcarb)}$, respectively (Table 3).

Table 1 The HOMO-LUMO energies and chemical reactivity descriptors (eV) of investigated compounds.

Compound	E_H	E_L	$\Delta E_{H\text{-}L}$	χ	η	δ	ω	Dipole
4a	−6.04	−3.24	**2.81**	4.64	1.40	0.71	7.67	6.27
4b	−5.82	−3.20	**2.62**	4.51	1.31	0.76	7.76	5.49
4c	−6.18	−3.37	**2.81**	4.77	1.40	0.71	8.11	6.17
6a	−5.83	−3.10	**2.73**	4.46	1.36	0.73	7.30	1.77
6b	−5.65	−3.06	**2.59**	4.36	1.30	0.77	7.32	0.86
6c	−5.96	−3.22	**2.74**	4.59	1.37	0.73	7.68	3.93

Table 2 The atomic Mulliken's charges of investigated compounds.

Atom	4a	4b	4c	6a	6b	6c
$N^1_{(Pp)}$	0.082	0.098	0.045	−0.020	−0.019	−0.029
$C^2_{(Pp)}$	−0.538	−0.544	−0.515	−0.544	−0.535	−0.522
$C^3_{(Pp)}$	0.124	0.068	0.112	0.166	0.086	0.133
$C^{3a}_{(Pp)}$	−0.484	−0.444	−0.498	−0.581	−0.539	−0.599
$N^4_{(Pp)}$	0.079	0.077	0.079	0.080	0.083	0.084
$C^5_{(Pp)}$	−0.111	−0.111	−0.114	−0.099	−0.069	−0.102
$C^6_{(Pp)}$	0.701	0.719	0.724	0.626	0.714	0.620
$C^7_{(Pp)}$	−0.344	−0.332	−0.361	0.254	0.161	0.266
$N^8_{(Pp)}$	−0.062	−0.082	−0.031	0.015	0.019	0.022
$NH_{(Pham)}$	0.138	0.145	0.139	0.124	0.136	0.129
$C^1_{(Pham)}$	0.038	0.017	0.059	0.130	0.078	0.158
$C^4_{(Pham)}$	−0.256	−0.255	−0.264	−0.263	−0.488	−0.272
$CO_{(carb)}$	−0.360	−0.326	−0.385	−0.417	−0.345	−0.403
$OC_{(carb)}$	−0.203	−0.203	−0.199	−0.207	−0.208	−0.205
$NH_{(carb)}$	0.143	0.133	0.119	0.128	0.127	0.115
$C^1_{(Phcarb)}$	−0.336	−0.538	−0.589	−0.267	−0.487	−0.545
$C^4_{(Phcarb)}$	0.673	−0.737	0.413	0.685	−0.718	0.406
$NH_{2(Pp)}$	−0.297	−0.297	−0.294	−0.426	−0.426	−0.425
$CN_{(Pp)}$	−0.895	−0.915	−0.907			
$NC_{(Pp)}$	−0.163	−0.162	−0.160			
$CO_{(carb1)}$				−0.435	−0.492	−0.450
$OC_{(carb1)}$				−0.316	−0.318	−0.315
$NH_{2(carb1)}$				−0.382	−0.387	−0.386
$Me_{(Phcarb)}$	−0.702	−0.527		−0.690		
$OMe_{(Phcarb)}$		−0.030			−0.032	
$Cl_{(Phcarb)}$			0.536			0.533

3.3. Biological evaluation

3.3.1. In vitro anticancer activity

In comparison to 5-fluorouracil (5-Fu), the cytotoxicity of six pyrazolo[1,5-*a*]pyrimidine compounds was examined across four cancer cell lines HepG2, Hep-2, PC3, MCF-7, and normal fibroblast cells (WI38) (Abd El-Meguid, Awad et al. 2019). Fig. 5 reflected the variations of cytotoxicity in expression of IC_{50}. Inspired the structural lineaments associated to anticancer activity are shown by the results of the investigated pyrazolopyrimidine compounds. The synthesized pyrazolo [1,5-*a*]pyrimidines revealed as a whole respectable cytotoxic effectiveness with distinct reactivity to hinder the growing of MCF-7 rather than Hep-2. Initially, 7-amino-*N*-aryl-6-cyano-2-(phenylamino)-pyrazolo[1,5-*a*]pyrimidine-3-carboxamide analogues **4a-c** were exhibited sensible inhibition activities toward MCF-7 (IC_{50} lies between 22.36 ± 0.23–29.42 ± 0.23 μM) than Hep-2 (IC_{50} lies between 16.78 ± 0.28–23.12 ± 0.45 μM), HepG2 (IC_{50} lies between 19.62 ± 0.13–25.61 ± 0.21 μM), and PC3 (IC_{50} lies between 29.36 ± 0.29–34.44 ± 0.53 μM) cell lines. Meanwhile, 7-Amino-2-(phenylamino)-pyrazolo[1,5-*a*]pyrimidine-3,6-dicarboxamides **6a-c** were displayed respectable cytotoxic effectiveness toward MCF-7 (IC_{50} lies between 10.80 ± 0.36–19.84 ± 0.49 μM) than Hep-2 (IC_{50} lies between 8.85 ± 0.24–12.76 ± 0.16 μM), HepG2 (IC_{50} lies between 26.81 ± 0.26–31.41 ± 0.05 μM), and PC3 (IC_{50} lies between 24.90 ± 0.29–26.90 ± 0.34 μM) cell lines.

3.3.2. Structural activity relationship

Rendering to cytotoxic outcomes of the prepared 7-amino-*N*-aryl-6-cyano-2-(phenylamino)-pyrazolo[1,5-*a*]pyrimidine-3-carboxamide analogues **4a-c**, it was perceived that 2-

Table 3 Selected top four atomic Fukui's indices, the local relative electrophilicity and nucleophilicity descriptors data of the investigated compounds.

4a		**4b**		**4c**		**6a**		**6b**		**6c**	
atom	f_k^-	**atom**	f_k^-	**atom**	f_k^-	**atom**	f_k^-	**atom**	f_k^-	**atom**	f_k^-
$NC_{(Pp)}$	0.058	$OMe_{(Phcarb)}$	0.064	$C^{1}_{(Phcarb)}$	0.077	$C^{4}_{(Pham)}$	0.058	$OMe_{(Phcarb)}$	0.057	$C^{1}_{(Phcarb)}$	0.069
$C^{4}_{(Pham)}$	0.055	$C^{1}_{(Phcarb)}$	0.050	$C^{4}_{(Pham)}$	0.058	$NH_{(Pham)}$	0.056	$C^{4}_{(Phcarb)}$	0.046	$C^{4}_{(Pham)}$	0.061
$NH_{(Pham)}$	0.051	$C^{4}_{(Phcarb)}$	0.050	$NC_{(Pp)}$	0.058	$C^{3}_{(Pp)}$	0.037	$C^{1}_{(Phcarb)}$	0.042	$NH_{(Pham)}$	0.059
$C^{4}_{(Phcarb)}$	0.040	$NC_{(Pp)}$	0.046	$NH_{(Pham)}$	0.054	$C^{4}_{(Phcarb)}$	0.036	$C^{3}_{(Phcarb)}$	0.040	$C^{3}_{(Pp)}$	0.038
$C^{3}_{(Pp)}$	0.033	$C^{3}_{(Pham)}$	0.045	$C^{3}_{(Pp)}$	0.035	$C^{2}_{(Pham)}$	0.033	$C^{2}_{(Phcarb)}$	0.037	$C^{2}_{(Pham)}$	0.035
atom	f_k^+	**atom**	f_k^+	**atom**	f_k^+	**atom**	f_k^+	**atom**	f_k^+	**atom**	f_k^+
$NC_{(Pp)}$	0.110	$NC_{(Pp)}$	0.112	$NC_{(Pp)}$	0.106	$C^{5}_{(Pp)}$	0.085	$C^{5}_{(Pp)}$	0.085	$C^{5}_{(Pp)}$	0.084
$C^{5}_{(Pp)}$	0.098	$C^{5}_{(Pp)}$	0.099	$C^{5}_{(Pp)}$	0.097	$OC_{(carb1)}$	0.075	$OC_{(carb1)}$	0.076	$OC_{(carb1)}$	0.071
$C^{3a}_{(Pp)}$	0.051	$C^{3a}_{(Pp)}$	0.052	$C^{3a}_{(Pp)}$	0.050	$CO_{(carb1)}$	0.059	$CO_{(carb1)}$	0.060	$CO_{(carb1)}$	0.055
$CN_{(Pp)}$	0.045	$CN_{(Pp)}$	0.047	$OC_{(carb)}$	0.046	$C^{3a}_{(Pp)}$	0.046	$C^{3a}_{(Pp)}$	0.046	$C^{3a}_{(Pp)}$	0.046
$N^{4}{}_{(Pp)}$	0.044	$N^{4}{}_{(Pp)}$	0.045	$Cl_{(Phcarb)}$	0.045	$N^{4}{}_{(Pp)}$	0.043	$N^{4}{}_{(Pp)}$	0.045	$Cl_{(Phcarb)}$	0.043
atom	f_k^0	**atom**	f_k^0	**atom**	f_k^0	**atom**	f_k^0	**atom**	f_k^0	**atom**	f_k^0
$NC_{(Pp)}$	0.084	$NC_{(Pp)}$	0.079	$NC_{(Pp)}$	0.082	$C^{5}_{(Pp)}$	0.054	$C^{5}_{(Pp)}$	0.052	$Cl_{(Phcarb)}$	0.056
$C^{5}_{(Pp)}$	0.061	$C^{5}_{(Pp)}$	0.059	$Cl_{(Phcarb)}$	0.061	$OC_{(carb1)}$	0.051	$OC_{(carb1)}$	0.049	$C^{5}_{(Pp)}$	0.054
$C^{4}_{(Pham)}$	0.039	$OMe_{(Phcarb)}$	0.040	$C^{5}_{(Pp)}$	0.060	$C^{4}_{(Pham)}$	0.041	$CO_{(carb1)}$	0.035	$OC_{(carb1)}$	0.049
$OC_{(carb)}$	0.038	$OC_{(carb)}$	0.039	$C^{4}_{(Pham)}$	0.041	$C^{3}_{(Pp)}$	0.037	$OC_{(carb)}$	0.035	$C^{4}_{(Pham)}$	0.042
$C^{3}_{(Pp)}$	0.037	$C^{4}_{(Phcarb)}$	0.034	$OC_{(carb)}$	0.038	$CO_{(carb1)}$	0.035	$OMe_{(Phcarb)}$	0.035	$C^{3}_{(Pp)}$	0.037
atom	S^+/S^-	**atom**	S^+/S^-	**atom**	S^+/S^-	**atom**	S^+/S^-	**atom**	S^+/S^-	**atom**	S^+/S^-
$C^{5}_{(Pp)}$	4.08	$C^{5}_{(Pp)}$	5.50	$CO_{(carb)}$	4.57	$CO_{(carb1)}$	4.92	$CO_{(carb1)}$	6.00	$CO_{(carb1)}$	4.58
$C^{3a}_{(Pp)}$	3.64	$C^{3a}_{(Pp)}$	4.73	$C^{5}_{(Pp)}$	4.04	$C^{5}_{(Pp)}$	3.70	$C^{5}_{(Pp)}$	4.72	$CO_{(carb)}$	4.14
$CO_{(carb)}$	3.38	$C^{2}_{(Pp)}$	4.40	$C^{3a}_{(Pp)}$	3.57	$CO_{(carb)}$	3.57	$C^{3a}_{(Pp)}$	3.83	$C^{5}_{(Pp)}$	3.65
$CN_{(Pp)}$	3.00	$CN_{(Pp)}$	4.27	$CN_{(Pp)}$	2.80	$C^{3a}_{(Pp)}$	3.29	$C^{2}_{(Pp)}$	3.67	$C^{3a}_{(Pp)}$	3.29
$N^{1}_{(Pp)}$	2.50	$N^{4}_{(Pp)}$	4.09	$N^{1}_{(Pp)}$	2.38	$OC_{(carb1)}$	2.78	$N^{4}_{(Pp)}$	3.46	$OC_{(carb1)}$	2.73
atom	S^+/S^-	**atom**	S^+/S^-	**atom**	S^+/S^-	**atom**	S^+/S^-	**atom**	S^+/S^-	**atom**	S^+/S^-
$C^{1}_{(Phcarb)}$	9.50	$C^{1}_{(Phcarb)}$	12.50	$C^{1}_{(Phcarb)}$	15.00	$C^{2}_{(Pham)}$	11.00	$C^{1}_{(Phcarb)}$	10.50	$C^{2}_{(Pham)}$	11.67
$C^{2}_{(Pham)}$	7.75	$C^{2}_{(Phcarb)}$	5.13	$C^{2}_{(Pham)}$	8.25	$C^{1}_{(Pham)}$	7.67	$C^{2}_{(Pham)}$	6.67	$C^{1}_{(Phcarb)}$	11.00
$C^{1}_{(Pham)}$	7.00	$OMe_{(Phcarb)}$	4.27	$C^{1}_{(Pham)}$	5.75	$C^{1}_{(Phcarb)}$	7.00	$C^{2}_{(Phcarb)}$	4.63	$C^{1}_{(Pham)}$	8.33
$NH_{(Pham)}$	4.25	$C^{2}_{(Pham)}$	4.25	$NH_{(Pham)}$	4.91	$NH_{(Pham)}$	5.09	$OMe_{(Phcarb)}$	4.07	$NH_{(Pham)}$	5.90
$C^{2}_{(Phcarb)}$	3.00	$C^{6}_{(Phcarb)}$	3.89	$C^{6}_{(Pham)}$	3.20	$C^{6}_{(Pham)}$	3.30	$C^{6}_{(Phcarb)}$	3.88	$C^{6}_{(Pham)}$	3.50

Table 4 Cytotoxic activity of synthesized and designed compounds against human tumor cell lines.

Compound	**Cytotoxicity IC_{50} (µM)**				
	Hep-2	**HepG2**	**PC3**	**MCF-7**	**WI38**
4a	23.12 ± 0.45	25.61 ± 0.21	34.44 ± 0.53	29.42 ± 0.23	26.15 ± 0.02
4b	19.82 ± 0.17	28.65 ± 0.43	37.64 ± 0.16	25.68 ± 0.16	34.64 ± 0.39
4c	16.78 ± 0.28	19.62 ± 0.13	29.36 ± 0.29	22.36 ± 0.23	35.18 ± 0.26
6a	12.76 ± 0.16	31.41 ± 0.05	26.19 ± 0.34	19.84 ± 0.49	32.47 ± 0.31
6b	10.71 ± 0.39	29.73 ± 0.66	24.90 ± 0.64	16.28 ± 0.11	37.26 ± 0.43
6c	8.85 ± 0.24	26.81 ± 0.26	26.37 ± 0.29	10.80 ± 0.36	42.64 ± 0.53
5-Fu	7.19 ± 0.47	5.33 ± 0.36	8.54 ± 0.23	10.19 ± 0.42	84.93 ± 0.28

5-Fluorouracil (5-Fu) is the known drug for antitumor assessments.

(phenylamino)-pyrazolo[1,5-*a*]pyrimidine-6-carbonitrile hybrids presented high grade of reactivity towards adenocarcinoma cell line (MCF-7) (Rahmouni, Souiei et al. 2016). However, hybrid **4c** (Ar = 4-ClC_6H_4) showed reasonable cytotoxic effectiveness with IC_{50} = 22.36 ± 0.23 µM toward against MCF-7 cell line, more than compound **4b** (Ar = 4-$MeOC_6H_4$) which demonstrated workable inhibition with IC_{50} = 25.68 ± 0.16 µM. However, the hybrid **4a** (Ar = 4-MeC_6H_4) revealed a little inhibition across MCF-7 with IC_{50} = 29.42 ± 0.23 µM. Meanwhile, the previous survey offered that 2-(phenylamino)-pyrazolo[1,5-*a*]pyrimidine-3-carboxamides displayed substantial effectiveness over (MCF-7) (Arias-Gómez, Godoy et al. 2021). Moreover, 7-Amino-2-(phenylamino)-pyrazolo[1,5-*a*]pyrimidine-3,6-dicarboxamide hybrid **6c** (Ar = 4-ClC_6H_4) demonstrated eminent effectiveness across MCF-7 with IC_{50} = 10.80 ± 0.36 µM. Furthermore, hybrid **6b** (Ar = 4-$MeOC_6H_4$) released pretty effectiveness with IC_{50} = 16.28 ± 0.11 µM, then hybrid **6a** (Ar = 4-MeC_6H_4) showed acceptable effectiveness across MCF-7 with IC_{50} = 19.84 ± 0.49 µM. In accordance to the literature survey, the

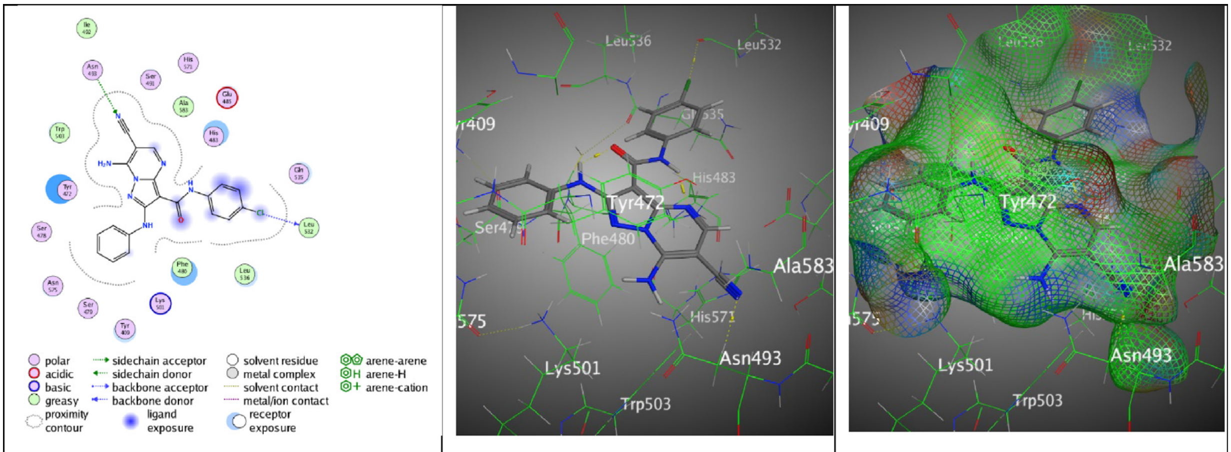

2D	3D	Surface Map

Fig. 5 The interaction between hybrid **4c** with (PDB ID: 5IVE).

order of anti-tumor effectiveness follows the arranging of hybrids to these findings: 4-OCH_3 > 4-Cl > 4-CH_3 (Abbas and Abd El-Karim 2019, Al-Anazi, Mahmoud et al. 2019). Additional examination of the prepared pyrazolo[1,5-*a*]pyrimidine hybrids was accomplished to realize their cytotoxic effectiveness on the normal cell fibroblast cells (WI38).

3.3.3. Molecular docking study

According to the scientific literature survey, new pyrazolo[1,5-*a*]pyrimidines have shown promise as KDM5A "histone lysine demethylase" inhibitors applied to treat breast cancer cells (Gehling, Bellon et al. 2016). These pyrazolo[1,5-*a*]pyrimidines possess structure like to ligand active site 5IVE. The finest structure of little tested compounds and the conformation of the KDM5A protein, that was recognized from (PDB- ID: 5IVE), were docked together (Metwally, Mohamed et al. 2019). The technique of docking progression was passed out to normalize the compound's preferred style of interrelating with the enzyme's active site. Meanwhile, the binding score (S, Kcal/mol) was utilized to compute the binding similarity of ligand over the enzyme active site; a low score of energy shows a good affinity. Through several prepared derivatives as a ligand and proteins as a target in a molecular docking simulation, the target-ligand interaction was located. The molecular docking study that was presented in Table 5, 7-amino-*N*-aryl-6-cyano-2-(phenylamino)-pyrazolo[1,5-*a*]pyrimidine-3-carboxamide analogues **4a-c** displayed adequate binding score S = -7.4318, −7.5101, and −7.9031 Kcal/mol, respectively (Table 5). Hybrids **4a** and **4b** exhibited the same H- acceptor bonds between Asn 493 with *N*-atom of nitrile moiety over intermolecular distances (3.63 and 3.39 Å) (Figures S1 and S2). Meanwhile, hybrid **4c** represented two H-bonds (H-donor and H-acceptor), Cl- atom with Leu 532 through (3.41 Å), N- atom of nitrile moiety with Asn 493 through (3.62 Å) (Fig. 5).

Meantime, 7-Amino-2-(phenylamino)-pyrazolo[1,5-*a*]pyrimidine-3,6-dicarboxamide derivatives **6a- 6c** revealed decent binding score S = -7.0158, −7.6607, and −8.0107 Kcal/mol, respectively. Hybrid **6a** displayed H- acceptor amongst O- atom of amide group with Asn 493 through (2.99 Å) (Figure S3). Meanwhile, compound **6b** displayed two H-bonds, H-donor among *N*-atom of amino moiety with Ser 491 through (2.91 Å), and H-acceptor between O-atom of amide substituent with Asn 493 through (3.04 Å) (Fig-

Table 5 Molecular docking data for the pyrazolo[1,5-*a*]pyrimidines analogues.

Code	S (Kcal/mol)	RMSD	Interaction with ligand	Types of Interactions	Distance (Å)
4a	−7.4318	1.0057	N- atom of nitrile moiety with Asn 493	H-acceptor	3.63
4b	−7.5101	0.9794	N- atom of nitrile moiety with Asn 493	H-acceptor	3.39
4c	−7.9031	0.9711	Cl- atom with Leu 532	H-donor	3.41
			N- atom of nitrile moiety with Asn 493	H- acceptor	3.62
6a	−7.0158	1.3333	O- atom of amide group with Asn 493	H-acceptor	2.99
6b	−7.6607	1.2059	N- atom of amide moiety with Ser 491	H-donor	2.91
			O- atom of amide moiety with Asn 493	H-acceptor	3.04
6c	−8.0107	1.0928	N- atom of amide moiety with Ser 491	H-donor	2.89
			O- atom of amide moiety with Asn 493	H-donor	3.30
			Cl- atom with Leu 532	H-acceptor	3.00
5-Fu	−4.2410	0.9567	O-atom of carbonyl moiety with Lys 501	H-acceptor	3.07
			Pyrimidine ring with Phe 480	π-π	3.70

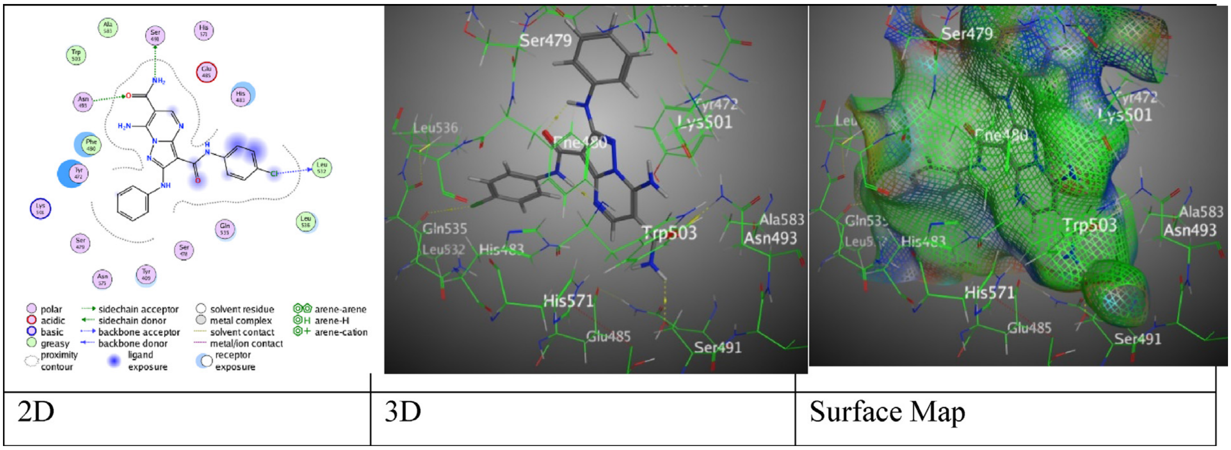

Fig. 6 The interaction between hybrid **6c** and (PDB ID: 5IVE).

ure S4). Moreover, compound **6c** revealed two H-donors among O-atom of amide substituent with Asn 493 through (3.30 Å), N- atom of amide moiety with Ser 491through (2.89 Å), and one H-acceptor between Cl- atom with Leu 532 through (3.00 Å) (Fig. 6).

Furthermore, 5-Fu presented H-acceptor among O-atom of carbonyl moiety with Lys 501 through (3.07 Å), and π-π attraction between pyrimidine ring with Phe 480 through (3.70 Å) through RMSD = 0.9567 with low score S = -4.2410 Kcal/mol (Figure S5).

Finally, the outcomes of molecular docking were presented the subsequent summaries: 1) the docking scores of the synthesized hybrids gave acceptable values ranged between −7.0158 to −8.0107 Kcal/mol. 2) 7-Amino-2-(phenylamino)- pyrazolo [1,5-*a*]pyrimidine-3,6-dicarboxamide hybrids **6a-c** were unveiled the furthermost many types of bindings like H-donor, H-acceptor, and π-π that offered superior confirmation for the best binding with the diverse amino-acids of 5IVE. 3) The synthesized hybrids were attached with the same amino-acids of protein over dissimilar polar and non-polar amino-acids like "Asn 493, and Leu 532" which presented good evidence for binding processes. 4) The resulted pictures of 2D, 3D, and surface map were reflected clear images of the close relationship between the synthesized ligands and the different types of 5IVE amino-acids.

4. Conclusion

A series of 7-amino-*N*-aryl-2-(phenylamino)pyrazolo[1,5-*a*]pyrimidine-3-carboxamide analogues **4** and **6** were obtained through cyclocondensation of 3-aminopyrzoles **2a-c** with 2-((dimethylamino)methylene)-malononitrile and/or 2-cyano-3-(dimethylamino)acrylamide. The DFT optimized structure of the investigated compounds indicated that all have almost planar configuration. All derivatives have similar HOMO and LUMO shapes and thus close $\Delta E_{H\text{-}L}$ gap was displayed, 2.59–2.81 eV, obeying the order **4a** = **4c** > **6c** ≈ **6a** > **4b** > **6b**. As well, the prepared 2-(phenylamino)-pyrazolo[1,5-*a*]pyrimidine derivatives demonstrated appropriate cytotoxic effectiveness with dissimilar activities to inhibit the growth of MCF-7 and Hep-2 cancer cell lines. Mainly, 7-amino-*N*-aryl-6-cyano-2-(phenylamino)-pyrazolo[1,5-*a*]pyrimidine-3-carboxamide analogues **4a-c** were revealed respectable cytotoxic effectiveness toward MCF-7 rather than the rest of cell lines through IC_{50} values (22.36 ± 0.23–29.42 ± 0.23 μM). Meanwhile, 7-Amino-2-(phenylamino)-pyrazolo[1,5-*a*]pyrimidine-3,6-dicarboxamide hybrids **6a-c** were revealed attentive inhibition over IC_{50} values against MCF-7 (10.80 ± 0.36–19.84 ± 0.49 μM) and Hep-2 (24.90 ± 0.29–26.90 ± 0.34 μM). All of the synthesized 2-(phenylamino)-pyrazolo[1,5-*a*] pyrimidine analogues were examined toward standard drug (5-Fu) with (IC_{50} = 7.19 ± 0.47 μM) for Hep-2 and (IC_{50} = 10.19 ± 0.42 μM) for MCF-7 in diminish to (WI38) normal cell. Moreover, the hypothetical outcomes of the molecular docking delivered acceptable approve over the findings of cytotoxic activity through the nominated (PDB Code-5IVE).

Declaration of Competing Interest

The authors declare that they have no known competing financial interests or personal relationships that could have appeared to influence the work reported in this paper.

Acknowledgement

The authors extend their appreciation to the Deanship of Scientific Research at King Khalid University for funding this work through Small Groups. Projects under grant number (RGP.1/102/43).

Appendix A. Supplementary material

Supplementary data to this article can be found online at https://doi.org/10.1016/j.arabjc.2022.104437.

References

Abbas, H.A.S., Abd El-Karim, S.S., 2019. Design, synthesis and anticervical cancer activity of new benzofuran–pyrazol-hydrazono-thiazolidin-4-one hybrids as potential EGFR inhibitors and apoptosis inducing agents. Bioorg. Chem. 89, 103035.

Abd El-Meguid, E., Awad, H., Anwar, M., 2019. Synthesis of new 1,3,4-oxadiazole-benzimidazole derivatives as potential antioxidants and breast cancer inhibitors with apoptosis inducing activity. Russ. J. Gen. Chem. 89 (348), 356.

Al-Anazi, K.M., Mahmoud, A.H., AbulFarah, M.A.A., et al, 2019. 2-Amino-5-arylazothiazole-based derivatives. in vitro cytotoxicity, antioxidant properties, and bleomycin-dependent DNA damage. ChemistrySelect 4, 5570 5576.

Al-Azmi, A., 2019. Pyrazolo[1,5-a]pyrimidines: a close look into their synthesis and applications. Curr Org. Chem. 23 (721), 743.

Alcolea Palafox, M., 2014. Anticancer drug IUdR and other 5-halogen derivatives of 2′-deoxyuridine: conformers, hydrates, and structure–activity relationships. Struct. Chem. 25 (53), 69.

Ali, G.M., Ibrahim, D.A., Elmetwali, A.M., et al, 2019. Design, synthesis and biological evaluation of certain CDK2 inhibitors based on pyrazole and pyrazolo[1,5-a]pyrimidine scaffold with apoptotic activity. Bioorg. Chem. 86 (1), 14.

Almehmadi, S.J., Alsaedi, A.M., Harras, M.F., et al, 2021. Synthesis of a new series of pyrazolo[1,5-a]pyrimidines as CDK2 inhibitors and anti-leukemia. Bioorg. Chem. 117, 105431.

Arias-Gómez, A., Godoy, A., Portilla, J., 2021. Functional pyrazolo [1,5-a]pyrimidines: current approaches in synthetic transformations and uses as an antitumor scaffold. Molecules 26, 2708.

Asano, T., Yamazaki, H., Kasahara, C., et al, 2012. Identification, synthesis, and biological evaluation of 6-[(6R)-2-(4-Fluorophenyl)-6-(hydroxymethyl)-4,5,6,7-tetrahydropyrazolo[1,5-a]pyrimidin-3-yl]-2-(2-methylphenyl) pyridazin-3(2 H)-one (AS1940477), a Potent p38 MAP kinase inhibitor. J. Med. Chem. 55 (7772), 7785.

Becke, A.D., 1993. Density-functional thermochemistry. III. the role of exact exchange. J. Chem. Phys. 98, 5648 5652.

Bhagyasree, J.B., Varghese, H.T., Panicker, C.Y., Samuel, J., et al, 2013. Vibrational spectroscopic (FT-IR, FT-Raman, (1)H NMR and UV) investigations and computational study of 5-nitro-2-(4-nitrobenzyl) benzoxazole. Spectrochim. Acta A Mol. Biomol. Spectrosc. 102 (99), 113.

Biovia, D.S., 2017. Materials Studio. Dassault Systèmes, San Diego.

Bouchoucha, A., Zaater, S., Bouacida, S.H., et al, 2018. Synthesis and characterization of new complexes of nickel (II), palladium (II) and platinum(II) with derived sulfonamide ligand: structure, DFT study, antibacterial and cytotoxicity activities. J. Mole. Struct. 1161 (345), 355.

Bulat, F.A., Chamorro, E., Fuentealba, P., et al, 2004. Condensation of frontier molecular orbital Fukui functions. J. Phys. Chem. A 108 (342), 349.

Burnett, M.E., Johnston, H.M., Green, K.N., 2015. Structural characterization of the aquaporin inhibitor 2-nicotinamido-1, 3, 4-thiadiazole. Acta Crystallogr. Sect. C: Struct. Chem. 71 (1074), 1079.

Castillo, J., Portilla, J., 2018. Recent advances in the synthesis of new pyrazole derivatives. Targets Heterocycl. Syst. 22 (194), 223.

Castillo, J.C., Rosero, H.A., Portilla, J., 2017. Simple access toward 3-halo-and 3-nitro-pyrazolo[1, 5-a]pyrimidines through a one-pot sequence. RSC Adv. 7 (28483), 28488.

Delley, B., 2006. Ground-state enthalpies: evaluation of electronic structure approaches with emphasis on the density functional method. J. Phys. Chem. A 110 (13632), 13639.

Eftekhari-Sis, B., Zirak, M., 2015. Chemistry of α-oxoesters: a powerful tool for the synthesis of heterocycles. Chem. Rev. 115 (151), 264.

El Adnani, Z., Mcharfi, M., Sfaira, M., et al, 2013. DFT theoretical study of 7-R-3methylquinoxalin-2 (1H)-thiones (RH;CH3;Cl) as corrosion inhibitors in hydrochloric acid. Corros. Sci. 68 (223), 230.

El Sayed, M.T., Hussein, H.A., Elebiary, N.M., et al, 2018. Tyrosine kinase inhibition effects of novel Pyrazolo[1,5-a]pyrimidines and Pyrido[2,3-d]pyrimidines ligand: Synthesis, biological screening and molecular modeling studies. Bioorg. Chem. 78 (312), 323.

Elgemeie, G.H., Elghandour, A.H.A., Elaziz, G.W., 2004. Potassium 2-Cyanoethylene-1-thiolate derivatives: a new preparative route to 2-Cyanoketene S, N-acetals and pyrazole derivatives. Synth. Commun. 34 (3281), 3291.

Elgemeie, G.H., Jones, P.G., 2004. 5-Amino-3-anilino-N-(chlorophenyl)-1H-pyrazole-4-carboxamide ethanol solvate. Acta Crystallogr. Sect. E: Struct. Rep. 60.

Frisch, M., Trucks, G., Schlegel, H., et al, 2009. Gaussian 09, Revision A. 1. Wallingford, CT, USA: Gaussian. .

Gehling, V.S., Bellon, S.F., Harmange, J.C., et al, 2016. Identification of potent, selective KDM5 inhibitors. Bioorg. Med. Chem. Lett. 26 (4350), 4354.

Jismy, B., Tikad, A., Akssira, M., et al, 2020. Efficient access to 3, 5-disubstituted 7-(Trifluoromethyl) pyrazolo[1,5-a]pyrimidines involving SN Ar and Suzuki cross-coupling reactions. Molecules 25, 2062.

Johnson, J.L., Khan, M.F., 2018. Biosynthetic pathways frequently targeted by pharmaceutical intervention. Fundam. Med. Chem. Drug Metab. 1 (281), 323.

Joshi, G., Nayyar, H., Marin Alex, J., et al, 2016. Pyrimidine-fused derivatives: synthetic strategies and medicinal attributes. Curr. Top. Med. Chem. 16 (3175), 3210.

Jubeen, F., Iqbal, S.Z., Shafiq, N., et al, 2018. Eco-friendly synthesis of pyrimidines and its derivatives: a review on broad spectrum bioactive moiety with huge therapeutic profile. Synth. Commun. 48 (601), 625.

Kumar, H., Das, R., Choithramani, A., et al, 2021. Efficient green protocols for the preparation of pyrazolopyrimidines. ChemistrySelect 6 (5807), 5837.

Lee, C., Yang, W., Parr, R.G., 1988. Development of the Colle-Salvetti correlation-energy formula into a functional of the electron density. Phys. Rev. B 37 (785), 789.

Liu, M.G., Liao, Q.B., 2006. Ethyl 5-(triphenylphosphoranylideneamino)-1H-1,2, 3-triazole-4-carboxylate. Acta Crystallograph. Section E: Struct. Rep. Online 62, o2214 o2215.

Lunagariya, M.V., Thakor, K.P., Waghela, B.N., et al, 2018. Design, synthesis, pharmacological evaluation and DNA interaction studies of binuclear Pt (II) complexes with pyrazolo [1,5-a] pyrimidine scaffold. Appl. Organomet. Chem. 32, e4222.

Mackman, R.L., Sangi, M., Sperandio, D., et al, 2015. Discovery of an oral respiratory syncytial virus (RSV) fusion inhibitor (GS-5806) and clinical proof of concept in a human RSV challenge study. ACS Publications J. Med. Chem. 58 (1630), 1643.

Mahapatra, A., Prasad, T., Sharma, T., 2021. Pyrimidine: A review on anticancer activity with key emphasis on SAR. Future J. Pharm. Sci. 7 (1), 38.

Makhlouf, M.M., Radwan, A.S., Ghazal, B., 2018. Experimental and DFT insights into molecular structure and optical properties of new chalcones as promising photosensitizers towards solar cell applications. Appl. Surf. Sci. 452 (337), 351.

Matyugina, E.S., Logashenko, E.B., Zenkova, M.A., et al, 2015. 5′-Norcarbocyclic analogues of furano [2,3-d] pyrimidine nucleosides. Heterocycl. Commun. 21 (259), 262.

Messali, M., Larouj, M., Lgaz, H., et al, 2018. A new schiff base derivative as an effective corrosion inhibitor for mild steel in acidic media: experimental and computer simulations studies. J. Mole. Struct. 1168, 39–48.

Metwally, N.H., Mohamed, M.S., Ragb, E.A., 2019. Design, synthesis, anticancer evaluation, molecular docking and cell cycle analysis of 3-methyl-4,7-dihydropyrazolo[1,5-a]pyrimidine derivatives as potent histone lysine demethylases (KDM) inhibitors and apoptosis inducers. Bioorg. Chem. 88, 102929.

Mi, H., Xiao, G., Chen, X., 2015. Theoretical evaluation of corrosion inhibition performance of three antipyrine compounds. Comput. Theor. Chem. 1072 (7), 14.

Mukhtar, S.S., Hassan, A.S., Morsy, N.M., et al, 2021. Design, synthesis, molecular prediction and biological evaluation of pyrazole-azomethine conjugates as antimicrobial agents. Synth. Commun. 51 (1564), 1580.

Nerkar, A.U., 2021. Use of pyrimidine and its derivative in pharmaceuticals: a review. J. Adv. Chem. Sci. 7 (729), 732.

Olasunkanmi, L.O., Obot, I.B., Ebenso, E.E., 2016. Adsorption and corrosion inhibition properties of N-{n-[1-R-5-(quinoxalin-6-yl)-4,5-dihydropyrazol-3-yl]phenyl}methane sulfonamides on mild steel in 1 M HCl: experimental and theoretical studies. RSC Adv. 6 (86782), 86797.

Perdew, J.P., Wang, Y., 1992. Pair-distribution function and its coupling-constant average for the spin-polarized electron gas. Phys. Rev. B 46 (12947), 12954.

Pinheiro, S., Pinheiro, E., Muri, E.M., et al, 2020. Biological activities of [1,2,4]triazolo[1,5-a]pyrimidines and analogs. Med. Chem. Res. 29 (1751), 1776.

Rahmouni, A., Souiei, S., Belkacem, M.A., et al, 2016. Synthesis and biological evaluation of novel pyrazolopyrimidines derivatives as anticancer and anti-5-lipoxygenase agents. Bioorg. Chem. 66 (160), 168.

Roy, R., De Proft, F.d., Geerlings, P., 1998. Site of protonation in aniline and substituted anilines in the gas phase: a study via the local hard and soft acids and bases concept. J. Physi. Chem. A 102, 7035 7040.

Roy, R., Krishnamurti, S., Geerlings, P., et al, 1998. Local softness and hardness based reactivity descriptors for predicting intra-and intermolecular reactivity sequences: carbonyl compounds. J. Phys. Chem. A 102 (3746), 3755.

Roy, R.K., Pal, S., Hirao, K., 1999. On non-negativity of Fukui function indices. J. Chem. phys. 110 (8236), 8245.

Sajan, D., Joseph, L., Vijayan, N., et al, 2011. Natural bond orbital analysis, electronic structure, non-linear properties and vibrational spectral analysis of L-histidinium bromide monohydrate: a density functional theory. Spectrochim. Acta Part A: Mole. Biomole. Spectrosc. 81, 85 98.

Salem, M.A., Helal, M.H., Gouda, M.A., et al, 2019. Recent synthetic methodologies for pyrazolo[1,5-a]pyrimidine. Synth. Commun. 49 (1750), 1776.

Sathisha, K., Gopala, S., Rangappa, K., 2016. Biological activities of synthetic pyrimidine derivatives. World J. Pharm. Res. 5 (1467), 1491.

Secrieru, A., O'Neill, P.M., Cristiano, M.L.S., 2019. Revisiting the structure and chemistry of 3 (5)-substituted pyrazoles. Molecules 25, 42.

Shirvani, P., Fassihi, A., Saghaie, L., 2019. Recent advances in the design and development of non-nucleoside reverse transcriptase inhibitor scaffolds. Chem. Med. Chem 14 (52), 77.

Taylor, A.I., Houlihan, G., Holliger, P., 2019. Beyond DNA and RNA: the expanding toolbox of synthetic genetics. Cold Spring Harb. Perspect. Biol. 11, a032490.

Tigreros, A., Aranzazu, S.L., Bravo, N.F., et al, 2020. Pyrazolo[1,5-a] pyrimidines-based fluorophores: a comprehensive theoretical-experimental study. RSC Adv. 10 (39542), 39552.

Tigreros, A., Macias, M., Portilla, J., 2021. Photophysical and crystallographic study of three integrated pyrazolo[1, 5-a]pyrimidine–triphenylamine systems. Dyes Pigm. 184, 108730.

Tigreros, A., Zapata-Rivera, J., Portilla, J., 2021. Pyrazolo[1,5-a] pyrimidinium salts for cyanide sensing: a performance and sustainability study of the probes. ACS Sustain. Chem. Eng. 9 (12058), 12069.

Tigreros, A., Macías, M., Portilla, J., 2022. Expeditious ethanol quantification present in hydrocarbons and distilled spirits: Extending photophysical usages of the pyrazolo[1,5-a]pyrimidines. Dyes Pigm. 202, 110299.

Xavier, S., Periandy, S., Ramalingam, S., 2015. NBO, conformational, NLO, HOMO–LUMO, NMR and electronic spectral study on 1-phenyl-1-propanol by quantum computational methods. Spectrochim. Acta Part A: Mole. Biomole. Spectrosc. 137, 306 320.

Xiaobao, C.B., Li, K., Shi, D.Q., 2008. Synthesis and crystal structure of N-(1,3,4-Thiadiazol-2-yl)-1-[1-(6-chloropyridin-3-yl)methy]-5-methyl-1H-[1,2,3]triazol-4-carboxamide. Chinese J. Struct. Chem. 27 (1389), 1392.

Zhao, M., Ren, H., Chang, J., et al, 2016. Design and synthesis of novel pyrazolo[1,5-a]pyrimidine derivatives bearing nitrogen mustard moiety and evaluation of their antitumor activity in vitro and in vivo. Eur. J. Med. Chem. 119 (183), 196.